
Article:
Pickering, E.J., Christofidou, K.A., Stone, H.J. et al. (1 more author) (2019) On the design and feasibility of tantalum-base superalloys. Journal of Alloys and Compounds, 804. pp. 314-321. ISSN 0925-8388

https://doi.org/10.1016/j.jallcom.2019.07.003

Journal of Alloys and Compounds 804 (2019) 314–321

Contents lists available at ScienceDirect

Journal of Alloys and Compounds

journal homepage: http://www.elsevier.com/locate/jalcom

On the design and feasibility of tantalum-base superalloys

E.J. Pickering [a, *], K.A. Christofidou [b], H.J. Stone [b], N.G. Jones [b]

[a] School of Materials, University of Manchester, Oxford Road, Manchester, M13 9PL, UK
[b] Department of Materials Science and Metallurgy, University of Cambridge, 27 Charles Babbage Road, Cambridge, CB3 0FS, UK

ARTICLE INFO

Article history:
Received 5 April 2019
Received in revised form
17 June 2019
Accepted 1 July 2019
Available online 4 July 2019

Keywords:
Superalloys
Refractory alloys
Tantalum alloys
Alloy design
High temperature alloys
Phase identification

ABSTRACT

In order to reduce the environmental impact of air travel, it is desirable that the efficiencies of gas turbine engines are increased. One way to achieve this goal is to increase the operating temperatures of the engine cores. Unfortunately for aero-engine manufacturers, the temperature capability limits of the Ni-base superalloys used currently have been reached. Hence, new alloys need to be developed that are capable of operating at significantly higher temperatures. In this article, the potential of tantalum-base superalloys is discussed and explored. A suite of alloys based on the Ta-Al-Co system was investigated. It was found that an array of fine carbide precipitates was formed in the Ta-rich matrix in a subset of the alloys, which is promising in terms of developing a strong and damage-tolerant microstructure, but that the elemental partitioning of Al out of the matrix accompanying precipitation is likely to degrade environmental resistance. Nevertheless, it is believed that the design principles described have the potential to facilitate the development of the next generation of high-temperature alloys based on systems of this type.

1. Introduction

As part of the global drive to reduce carbon emissions, the European Commission has laid out ambitious targets for the aviation industry, requiring the aircraft of 2050 to produce 75% less CO_2 per passenger kilometre than those of 2000 [1]. Increasing the thermodynamic efficiency of gas turbine engines will help meet this target, and this can be achieved by raising the operating temperature of the core engine stages. However, the alloys currently used in the hottest section, Ni-base superalloys, are working at the limit of their capabilities, which is inhibiting the development of higher-efficiency engines. Therefore, new materials are required to enable the development of the next generation of civil aerospace engines.

Over the last 60 years, Ni-base superalloys have enabled successive generations of gas turbine engines to operate at increasingly higher temperatures [2]. The success of these alloys has been based around their two-phase microstructures, which comprise small coherent ordered precipitates in a ductile FCC matrix. In addition, these alloys also have sufficient concentrations of scale-forming elements such that protective oxides layers develop at elevated temperatures. Nevertheless, despite continued research efforts to further develop these materials, progress has become incremental as they have approached the fundamental limits of their operation. Therefore, to facilitate a step change in operating temperature, it is necessary to consider entirely new alloy systems based on metallic elements with higher melting points.

2. Design philosophy

When considering the requirements of high-temperature materials for gas turbine engines, it is essential to have the correct balance of properties. Some of the most important of these are high creep strength, good environmental resistance, and adequate toughness, all of which must be sustained for prolonged periods in service.

The high-temperature mechanical properties of an alloy are dominated by the melting temperature (T_m) and crystal structure of the principal element. For a target temperature above the capability of Ni-base alloys, $\approx 1100\,^{\circ}C$, adequate creep resistance will likely require FCC or HCP elements with $T_m \gtrsim 1800\,^{\circ}C$ or BCC elements with $T_m \gtrsim 2500\,^{\circ}C$, owing to the increased diffusivity of BCC crystals [3–5]. This restricts the potential base elements to 11 candidates: Nb, Mo, Tc, Ru, Rh, Ta, W, Re, Os, Ir and Pt. However, if terrestrial abundance and cost are considered, the BCC refractory metals Nb, Mo, Ta and W alone remain the only viable options.

* Corresponding author.
E-mail address: ed.pickering@manchester.ac.uk (E.J. Pickering).

https://doi.org/10.1016/j.jallcom.2019.07.003

Environmental resistance above 1000°C can be afforded by forming silica (SiO_2) or alumina (Al_2O_3) protective scales; the effectiveness of chromia (Cr_2O_3) is diminished at such temperatures. Alumina is preferred as it is compatible with current coating technologies and is less sensitive to atmospheres containing water vapour [6,7]. Thus, significant concentrations of Al are desirable in the matrix of any new alloy in order to confer environmental resistance.

As demonstrated by Ni-base superalloys, significant strengthening and damage tolerance can be achieved by incorporating intermetallic precipitates within a metallic solid solution matrix. Further creep resistance and stability can be achieved if these precipitates are small, have a crystal structure which is a superlattice of the matrix, and are highly coherent. The superlattice structures of BCC structure (A2 in Strukturbericht notation) are B2 (CsCl), $D0_3$ (half-Heusler) and $L2_1$ (Heusler). However, there are no binary refractory metal-aluminium alloy systems that contain a two-phase field between an A2 phase and a corresponding A2 superlattice phase [8] and so any new alloy requires, at minimum, a ternary-base system.

The simplest option in a ternary system is to search for suitable binary superlattice compounds that might be compatible with a refractory metal solid solution. This approach was used by Ghosh et al. [9] to successfully create two-phase A2-B2 and A2-$L2_1$ microstructures. However, the coherency between the matrix and precipitate phases was low, with lattice misfits >6%. Furthermore, the intermetallic phases were based on the ternary element, and therefore required a two-phase field that traversed wide regions of compositional space, potentially limiting the volume fraction of superlattice precipitates that can form.

An alternative approach, which would narrow the two-phase region between matrix and precipitate, is to look for ternary refractory-metal-containing intermetallic compounds that are superlattices of the A2 phase. A search for such compounds revealed phases based on the ternary addition, such as Co_2TaAl (a Heusler compound with $CuHg_2Ti$-type structure) [10]. However, none of these phases exist in equilibrium with a refractory metal solid solution. RM-Al-X systems are poorly characterised in general, particularly in the refractory-metal-rich corner of compositional space.

A study by Hunt and Raman attempted to characterise the phases present in a number of Ta-Al-X and Nb-Al-X ternary systems [11]. They reported a new RM-rich ternary intermetallic phase in both the Ta-Al-Co and Nb-Al-Co systems, designated μ', but did not determine the crystal structure fully. The existence of this phase is interesting, since its chemistry was found to be close RM_2CoAl, a stoichiometry that could be consistent with a superlattice structure. Dovbenko et al. [12] were unable to find μ' in their recent study of the Nb-Al-Co system, but the existence of this phase has not been further investigated in the Ta-Al-Co system. Therefore, the present study sought to ascertain the phase equilibria in the Ta-rich corner of the Ta-Al-Co system, and provide an assessment of its suitability as a potential basis for tantalum-base superalloys.

3. Experimental

Three Ta-Al-Co alloys were prepared as ingots weighing 40 g via arc melting in an inert atmosphere from elemental metals with 99.95% purity using a tungsten electrode. To minimise compositional inhomogeneity, the ingots were inverted and remelted fifteen times. Short sections of each ingot, approximately 10 mm long, were cut from the as-cast ingots, encapsulated in an evacuated argon-backfilled quartz ampoule, and heat treated at either 1300°C or 1000°C for 500 h, before quenching in water. They were subsequentally sectioned and prepared for analysis using standard metallographic techniques.

Table 1
Composition of alloys investigated as determined by SEM EDX area analyses. Concentrations in at%. Error is one standard deviation in five measurements.

Label		Ta	Al	Co
TAC15	Nominal	70	15	15
	Measured	70.2 ± 0.8	13.7 ± 0.5	16.2 ± 0.8
TAC20	Nominal	60	20	20
	Measured	65.2 ± 0.5	14.9 ± 0.2	20.1 ± 0.4
TAC25	Nominal	50	25	25
	Measured	54.7 ± 0.2	20.2 ± 0.4	25.1 ± 0.3

Bulk compositional analyses were performed using energy-dispersive X-ray spectroscopy (EDX) on a JEOL 5800 scanning electron microscope (SEM). The compositions quoted in Table 1 are an average of five independent measurements from 500 μm × 500 μm areas. It is evident that some Al was lost during the melting process, but the alloy compositions still traverse the region of compositional space that is of interest.

Back-scattered electron (BSE) images and EDX elemental maps were acquired on either an FEI Nova NanoSEM or an FEI Sirion SEM. Foils for transmission electron microscopy (TEM) were prepared by focussed ion beam (FIB) milling using an FEI Nova 600 NanoLab DualBeam FIB/SEM. Selected-area electron diffraction patterns (SADPs) were taken using an FEI Tecnai Osiris or an FEI Talos F200X microscope, both with an accelerating voltage of 200 kV. The same microscopes were also used for scanning TEM (STEM) imaging using a high-angle annular dark-field (HAADF) detector, as well as energy-dispersive X-ray mapping in STEM mode (STEM-EDX).

4. Results

4.1. 1300°C for 500 h

After heat treatment at 1300°C for 500 h, the microstructures of both TAC15 and TAC20 comprised three distinct phases, Fig. 1. These differed in terms of their back-scattered signal, one appearing white (brightest), one grey (intermediate), and one black (darkest). They are labelled as A (white), B (grey) and C (black) in Fig. 1a–b. The chemistries of each phase were obtained using five EDX point analyses, and their averages are given in Table 2. These compositions are consistent with the back-scattered signal – the brighter phases appearing richer in heavier elements. The grey and black phases have a similar Ta content, but vary in their Al and Co concentrations. These variations are further demonstrated through the elemental map shown for TAC15 in Fig. 2, in which the phases are also labelled. The change in contrast that can be observed in phase A in Fig. 1a–b was not found to be associated with any change in chemistry, and was consistent with that associated with different grain orientations. The TAC25 alloy was found to contain one phase only, which was consistent with the grey Co-rich phase B observed in TAC15 and TAC20. The contrast in Fig. 1c is crystallographic and no compositional variations were detectable between regions of different brightness.

TEM SADPs were taken from each of the three phases in TAC15 and TAC20, as well as from the single B phase present in TAC25. Examples of the diffraction patterns obtained from each phase in TAC15 are shown in Fig. 3; these patterns are also representative of the same phases in TAC20 and TAC25. Surprisingly, the SADPs from the white Ta-rich phase A, Fig. 3a–b, were not consistent with a BCC solid solution as might have been expected, but instead matched the Ta_2Al tetragonal σ phase (CrFe prototype structure), with approximate lattice parameters of $a = b \approx 9.7$ Å and $c \approx 5.1$ Å. Low index zone axis SADPs from the grey Co-rich phase B in Fig. 3c–d were consistent with the previously-reported Ta_6Co_7 μ phase [11],

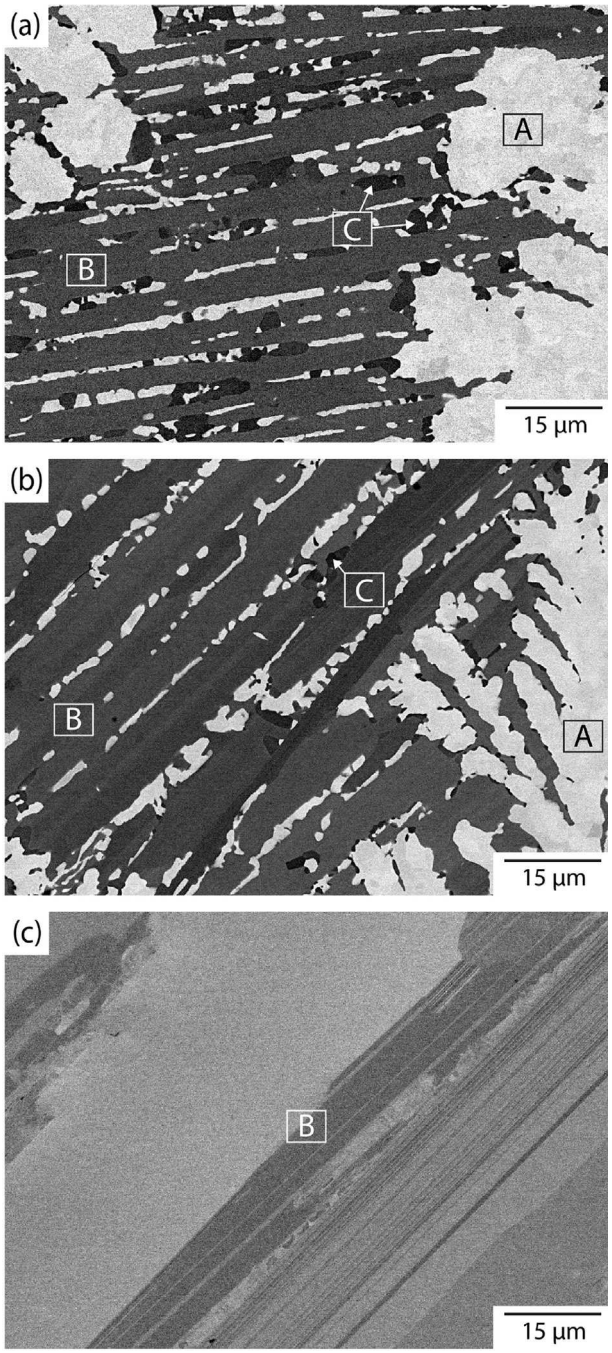

Fig. 1. BSE images of (a) TAC15, (b) TAC20 and (c) TAC25, all after heat treatment of 500 h at 1300°C.

Table 2
Composition of the three phases identified in the TAC alloys after exposure at 1300°C for 500 h, as determined by SEM EDX point analyses. Concentrations in at%. Error is one standard deviation in five measurements.

Label	BSE contrast	Alloy	Ta	Al	Co
A	White	TAC15	80.9 ± 0.2	7.7 ± 0.2	11.5 ± 0.3
		TAC20	80.7 ± 0.2	7.3 ± 0.3	11.5 ± 0.2
B	Grey	TAC15	59.6 ± 0.3	15.2 ± 0.3	25.2 ± 0.4
		TAC20	58.9 ± 0.3	15.9 ± 0.3	25.2 ± 0.4
		TAC25	54.5 ± 0.5	25.1 ± 0.4	20.4 ± 0.3
C	Black	TAC15	58.3 ± 0.7	23.5 ± 0.7	18.2 ± 0.5
		TAC20	58.0 ± 0.2	23.4 ± 0.3	18.6 ± 0.4

which has the W_6Fe_7 hexagonal prototype structure, but SADPs from other high index poles could not be indexed to this structure. The approximate lattice parameters for this phase were found to be $a = b \approx 5.0$ Å and $c \approx 27.2$ Å assuming hexagonal symmetry. SADPs from the dark Al-rich phase demonstrated that it had an FCC structure with a large lattice parameter of $a \approx 11.6$ Å, Fig. 3e–f. These matched the carbide Ta_3Al_2CoC [13,14].

5. 1000°C for 500 h

Fig. 4 shows BSE images of the three alloys following heat treatment at 1000°C for 500 h. From back-scatter contrast, a mixture of four phases appear to be present in TAC15 and TAC20, whilst TAC25 shows two phases. On comparison to Fig. 1, it is apparent that a precipitation event has occurred in the Ta-rich phase A in both TAC15 and TAC20, producing a matrix phase (labelled phase D) that appears a more brighter white than phase A, and a population of precipitates with dark back-scattered contrast.

From TAC15 and TAC25, the chemistries of the phases were obtained using at least five EDX point analyses, and their averages are given in Table 3. As indicated, the chemistries (and appearances) of two of the phases were consistent with phase A and phase B observed during ageing at 1300°C. The mixture of phase D and precipitate is similar to that of phase A. The chemistry of phase D, nor the chemistry of the precipitate in phase D, could be isolated owing to their size (similarly, neither could the phase with the darkest BSE contrast in Fig. 4a, b & d). The high uncertainty quoted with measurements for phase A are indicative of compositional variation seen in this phase and is likely due to the diminished size of these regions in this condition (and hence interference from different phases within the EDX interaction volume). The high uncertainty for the mixture of D and precipitate is likely due to their mixed nature meaning different fractions of each were sampled with each point.

Fig. 5 shows STEM bright-field and HAADF images of TAC20 aged at 1000°C for 500 h, alongside STEM-EDX results. A comparison to Fig. 2 shows that the chemical partitioning is similar to that present in material aged at 1300°C. This indicated the presence of phases A, B and C, with phase C being that with the darkest back-scatter contrast in Fig. 4a, b & d. This was confirmed with selected area electron diffraction. The precipitates in phase D were also found to have composition and crystal structure consistent with phase C. Phase D was found to be richer in Ta than phase A, but the STEM HAADF contrast of phase D is not as bright as for phase A, despite the Ta enrichment. This is perhaps due to the different crystal structures involved, but could also be a result of the presence of fine-scale features in D, shown in Fig. 6. Many of these features appear to be small precipitates of phase C, although the presence of dislocations and/or strain is also likely (possibly from the FIB preparation).

The identity of phase D, as well as the crystallographic relationship between phase C (Ta_3Al_2CoC) and phase D, was investigated. Phase D was found to be BCC with a lattice parameter $a \approx 3.3$ Å, consistent with a Ta-base BCC solid solution phase. As shown in Fig. 7, a crystallographic relationship was found between the two phases. The SADPs acquired implied the following orientation relationship:

$$[112]_{Ta_3Al_2CoC} \text{near to } [111]_{Ta}$$

$$(11\bar{1})_{Ta_3Al_2CoC} \text{near to} (1\bar{1}0)_{Ta}$$

$$(\bar{1}10)_{Ta_3Al_2CoC} \text{near to} (11\bar{2})_{Ta}$$

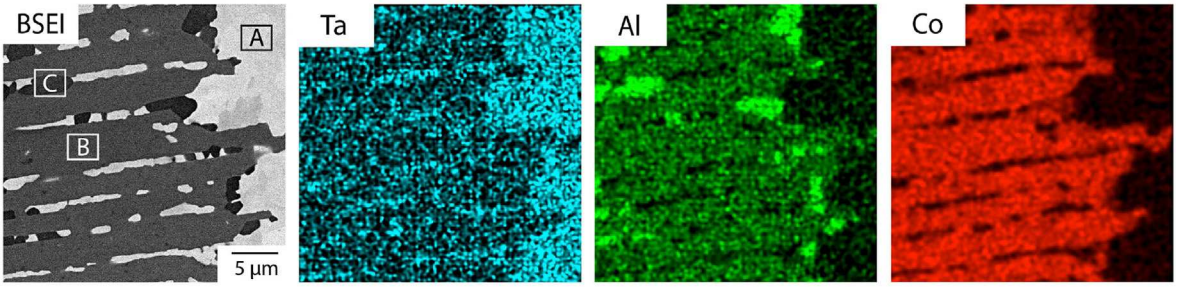

Fig. 2. SEM BSE image and SEM EDX elemental distribution maps for an area of TAC15 (1300°C for 500 h). It is clear that three distinct phases are present, A, B and C, each with different back-scatter contrasts and chemical compositions.

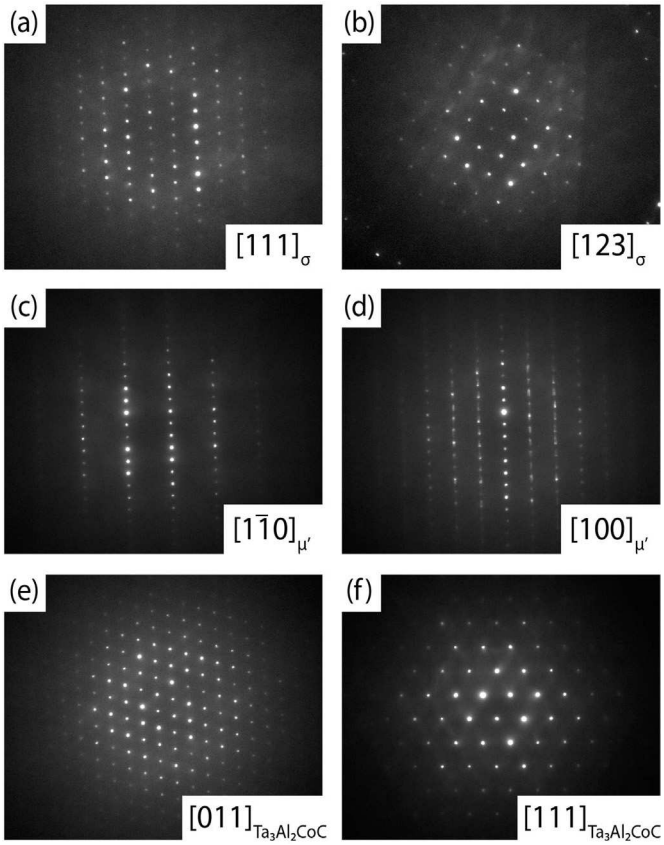

Fig. 3. TEM SADPs taken from TAC15 (1300°C for 500 h): a-b Ta-Rich phase A, c-d Co-rich phase B, e-f Al-rich phase C.

An angle of rotation of 1–3° appeared to bring the $[112]_{Ta_3Al_2CoC}$ and $[111]_{Ta}$ directions into coincidence, with the axis of rotation close to $[11\bar{2}]_{Ta}$ ($[\bar{2}20]_{Ta_3Al_2CoC}$) (left-handed rotation). This orientation relationship is consistent with the Greninger-Troiano orientation relationship between FCC and BCC phases [15], which is also close to the Nishiyama-Wassermann orientation relationship [16–18]. The following plane spacing relationships can also be observed in Fig. 7: $3d_{110,Ta} \approx d_{111,Ta_3Al_2CoC}$, and $3d_{112,Ta} \approx d_{220,Ta_3Al_2CoC}$. These are in agreement with the lattice parameters $a \approx 11.6$ Å for FCC Ta_3Al_2CoC phase C and $a \approx 3.3$ Å for BCC Ta phase D.

As regards the two phases present in the TAC25 sample, EDX results (Table 3) indicated that the phase with lighter back-scatter contrast (the majority phase) was phase B, and this was confirmed by selected-area electron diffraction (reflections in the low-index patterns collected matched the Ta_6Co_7 μ phase [11]). The second phase, with darker back-scattered contrast, did not match any of the phases A-D, and appeared to be leaner in Ta and richer in Co and Al than any of the other phases. This was labelled phase E. SADPs from this phase, Fig. 8, were consistent with a C14 Laves phase ($MgZn_2$ type structure), with approximate lattice parameters $a = 4.8$ Å and $c = 7.2$ Å.

6. Discussion

6.1. Phase identification

The phases identified by the present study are listed in Table 4. Three phases, labelled A, B and C were observed after ageing at 1300°C, whilst fives phases, A, B, C, D and E were found at 1000°C. The chemistries of these phases are given in Table 2 and A, B, D and E are marked on the reported Ta-Al-Co ternary phase diagram at 1000°C shown in Fig. 9 [11].

It is clear that not all the measured chemistries are obviously correlated with the phase fields reported before. Phase E certainly matches the C14 Laves phase space identified by Hunt and Raman [11], and phase B coincides relatively well with the μ' region. However, phase A has been identified as σ, so it would appear as though the σ phase region may extend to higher Co and Ta concentrations than previously reported. However, since temperatures high enough to eliminate microsegregation from casting could not be reached in this study, the microstructures observed here cannot be considered to be equilibrium ones. Furthermore, the presence of some contamination (clearly carbon was present to produce phase C), should also be noted. Each phase identified will now be discussed below.

Phase A: It is somewhat surprising that this Ta-rich phase was not found to be a BCC solid solution, since one would expect a phase with over 80 at.% Ta to form such a structure. Nevertheless, the results of electron diffraction confirmed that its structure was that of a Ta_2Al σ phase, and the propensity of the phase to crack (see Figs. 4d and 5) is consistent with the limited ductility of σ intermetallics. On the basis of this result, it is clear that the Ta_2Al has a higher solubility for Co than Fig. 9 suggests. This result is supported by the work performed by Dovbenko et al. [12] examining the Nb-Al-Co system, in which it was found that the solubility of Co in Nb_2Al was in excess of 11.4 at.%.

Phase B: It was initially believed, on the basis of low-index diffraction patterns like those in Fig. 3c–d, that this phase had the μ crystal structure. However, other high-index SADPs obtained from the phase could not be indexed to μ, and its chemistry was found to be more Ta-rich than would be expected from μ. Indeed, its chemistry was found to coincide closely with the μ' phase reported by Hunt and Raman [11], Fig. 9, and its characteristics most closely align to this phase. It seems that Hunt and Raman [11] named the

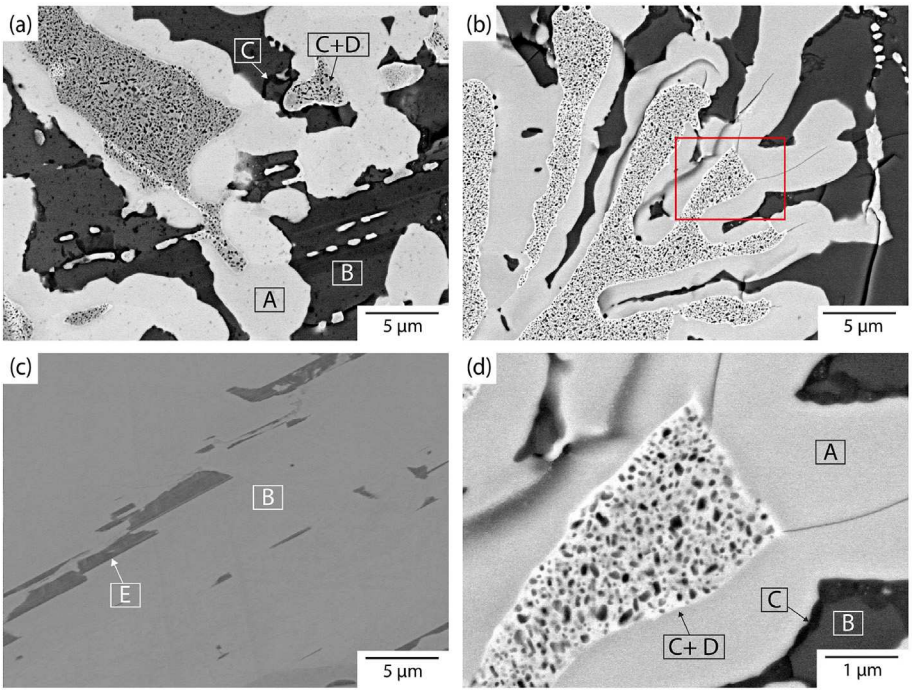

Fig. 4. SEM BSE images of (a) TAC15, (b) TAC20 and (c) TAC25, all after heat treatment of 500 h at 1000°C. (d) shows the region boxed in (b) at higher magnification.

Table 3
Composition of the three phases identified in the TAC alloys after exposure at 1000°C for 500 h, as determined by SEM EDX point analyses. Concentrations in at%. Error is one standard deviation in at least five measurements.

Label	BSE contrast	Alloy	Ta	Al	Co
A	White	TAC15	82.1 ± 6.8	5.1 ± 2.0	12.8 ± 4.8
		TAC20	77.1 ± 0.8	7.6 ± 0.5	15.3 ± 0.5
B	Grey	TAC15	53.8 ± 0.2	24.1 ± 0.6	22.1 ± 0.8
		TAC20	56.4 ± 0.3	20.6 ± 0.4	23.0 ± 0.4
		TAC25	51.9 ± 0.5	24.8 ± 0.2	23.2 ± 0.6
Mixture of matrix D	Brilliant white	TAC15	80.3 ± 5.8	6.2 ± 2.0	13.5 ± 3.8
+ ppt (C)	+ dark	TAC20	80.1 ± 2.1	7.4 ± 0.7	12.5 ± 1.3
E	Dark grey	TAC25	40.4 ± 1.1	30.4 ± 0.9	29.2 ± 0.5

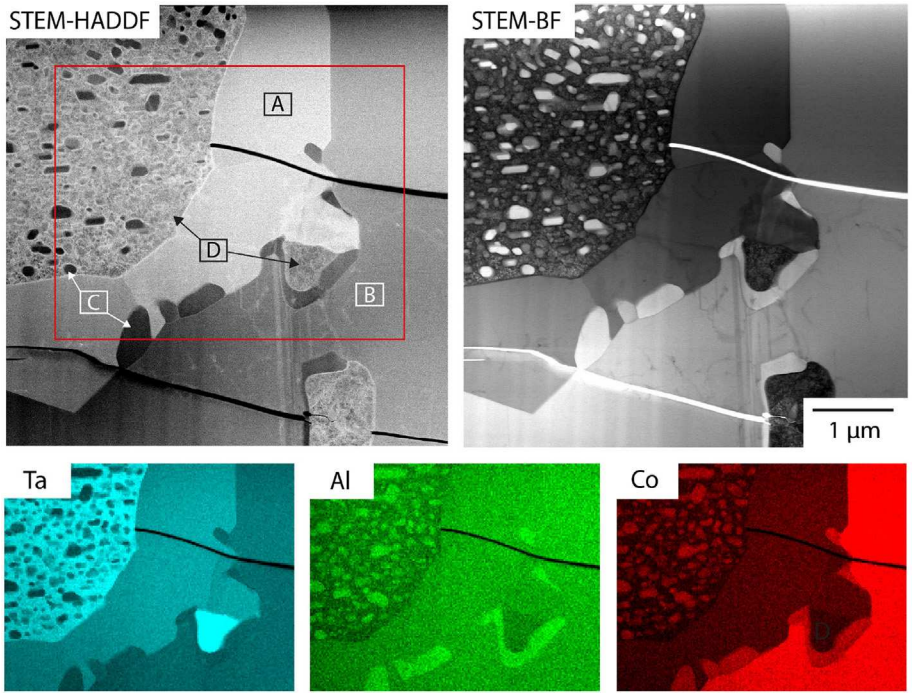

Fig. 5. STEM BF and HAADF images and STEM EDX elemental distribution maps of TAC20 aged at 1000°C for 500 h.

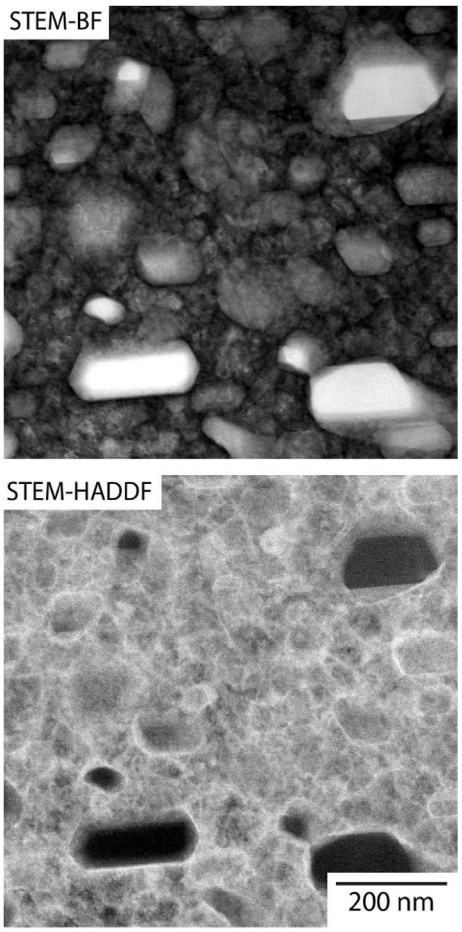

Fig. 6. STEM BF and HAADF images of precipitates of phase C (Ta_3Al_2CoC) formed in phase D (BCC Ta) in TAC20 aged at 1000°C for 500 h.

phase μ' in recognition of its similarity to μ, but could not elucidate its structure in full (as was the case in this study). It is interesting to note that the structure of the analogous phase in the Nb-Al-Co system, Nb_2AlCo, also has not be identified [8].

Phase C: This phase is a carbide, Ta_3Al_2CoC, which belongs to the family of η-carbides [14]. Its presence indicates that some carbon contamination was present in the alloys, most likely arising from the pure elements procured for their production. The reason why this phase did not arise in TAC25 after ageing at 1000°C appears to be because it only forms when the BCC phase D arises from decomposition of the σ phase A, and TAC25 contained no σ phase. Assuming a homogeneous contamination of carbon, results indicate that the σ phase A, μ' phase B and C14 Laves phase E all have some solubility for the carbon present, but that the solubility in the BCC phase D is more limited.

Phase D: This BCC solid-solution phase was not found in the alloy heat treated at 1300°C. It was not possible to quantify the composition of phase D directly by taking EDX spot analyses (in the TEM or SEM) because of concerns associated with interactions with surrounding precipitates and/or the unidentified fine-scale features in Fig. 6. Nevertheless, the STEM-EDX results in Fig. 5 suggest it is richer in Ta and leaner in Al and Co than phase A.

Phase E: The precipitation of this phase from phase B (μ') at 1000°C suggests there being more limited solubility for Co and Al in μ' than at 1300°C. Hunt and Raman noted the likely presence of a C14 Laves phase in their study (see Fig. 9), which is consistent with the crystal structure observed in SADPs of phase E.

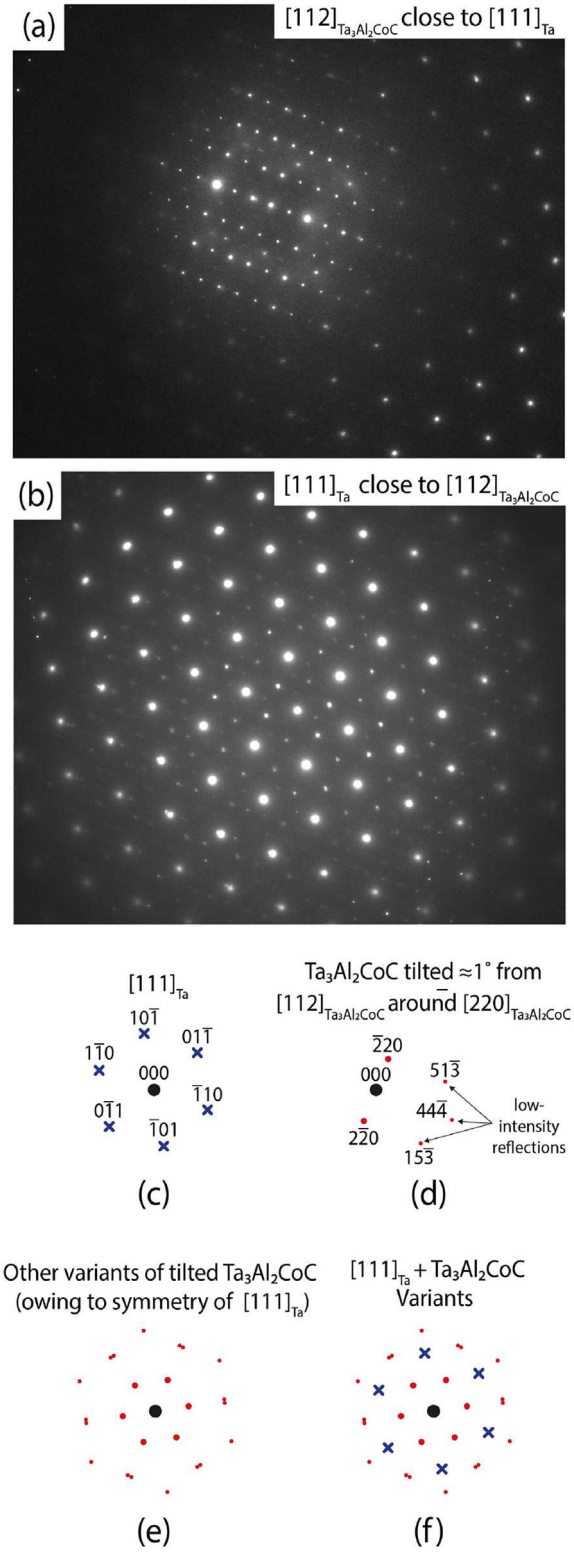

Fig. 7. TAC20 aged at 1000 for 500 h: (a) and (b) show the TEM SADPs taken down $[112]_{Ta3Al2CoC}$ (phase C, precipitate) and $[111]_{Ta}$ (phase D, matrix), respectively, with only a small tilt between the two. (c) shows the modelled electron diffraction pattern $[111]_{Ta}$ and (d) shows that from $[112]_{Ta3Al2CoC}$ tilted ≈1° around $[220]_{Ta3Al2CoC}$ ([112] Ta). (f) shows the superposition of six variants of the tilted $[112]_{Ta3Al2CoC}$ on $[111]_{Ta}$ to create the pattern seen in (b).

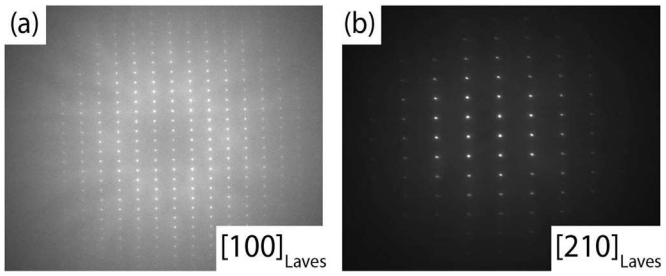

Fig. 8. TEM SADPs taken from phase E found in TAC25 aged at 1000°C for 500 h.

Table 4
Phase identification information. The nominal compositions (given in at.%) are approximate, based on the EDX data acquired. The lattice parameters are also approximate, having been obtained from electron diffraction.

Label	BSE Colour	Ta	Al	Co	Name	Crystal structure	Lattice parameters (Å)
A	White	81	8	12	σ	Tetragonal	$a \approx 5.2$, $c \approx 9.7$
B	Grey	55 −60	15 −25	20 −25	μ'	Hexagonal	$a \approx 5.0$, $c \approx 27.2$
C	Black	58	23	18	Ta_3Al_2CoC	FCC	$a \approx 11.6$
D	Brilliant white	? (>81)	? (<8)	? (<12)	Ta	BCC	$a \approx 3.3$
E	Dark grey	40	30	29	Laves	C14 Hexagonal	$a \approx 4.8$, $c \approx 7.2$

Going from 1300°C to 1000°C, the observations made here suggest that, for a sizeable portion of the phase A present at 1300°C, there is an overall change A→C + D. Given the morphological relationship between phases C and D, it is clear that phase C has precipitated in phase D, and that the transformation sequence was likely A→D→C + D (rather than a eutectoid reaction). Precisely how the transformation A→D occurs has not been probed in this report. It seems odd that a simply-structured solid solution (BCC phase D) would be unstable with respect to a more complex phase (phase A) at higher temperatures. The presence of carbon contamination may have influenced this.

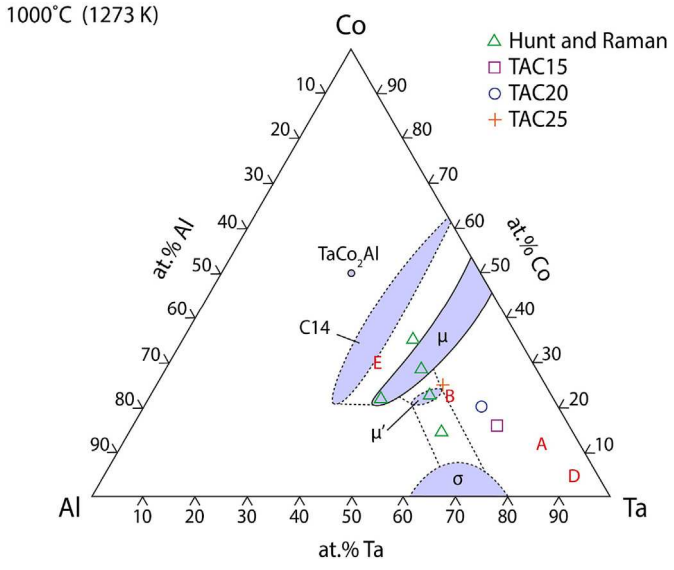

Fig. 9. Ta-Al-Co ternary phase diagram, redrawn using information from Refs. [8,11]. The alloys of Hunt and Raman are labelled with triangles, with the dashed lines denoting hypothesised phase boundaries [11]. The Ta-rich alloy compositions investigated in this study are marked, as are the compositions of the phases A, B, D and E identified.

The orientation relationship found between FCC phase C and BCC phase D was not the cube-cube type orientation relationship that had been hoped for, which would have been possible for superlattice B2 or Heusler precipitates. The discovery of a Greninger-Troiano [15] orientation relationship (or one close to it) between phases C and D is not unexpected, given the propensity of close-packed directions in the FCC and BCC phases to align during precipitation reactions.

6.2. Alloy design outlook

It is positive that a RM matrix + ternary precipitate combination has been observed in the Ta-Al-Co system, even if it is not the superlattice combination that had been hoped for. There are indications (i.e., the arresting of cracks) that suggest that this microstructure could have some damage tolerance, and it seems reasonable to suggest that the size and distribution of precipitates could be tailored through the heat treatment process. A somewhat unfortunate aspect of the formation of the phase C (Ta_3Al_2CoC) in D is that the Al partitions preferentially to the carbide. This is likely to limit resistance to environmental degradation, since a protective film cannot be formed from the matrix. Nevertheless, the investigations herein illustrate that the methodology to find candidate systems for refractory-metal-base superalloys shows some promise.

7. Summary and conclusions

- A summary of a strategy to design refractory-metal-base superalloys for high-temperature service has been described.
- The Ta-rich side of the Ta-Al-Co system has been investigated to determine whether an A2/A2-superlattice microstructure could be found.
- No precipitates with an A2-based superlattice structure were found, although fine precipitates of the carbide Ta_3Al_2CoC were found in a Ta-rich BCC solid solution matrix after ageing at 1000°C. These had a consistent orientation relationship with the matrix.
- Unfortunately, Al partitioned from the matrix to the Ta_3Al_2CoC, which will limit the environmental resistance of the alloy. Nevertheless, there were indications that the combination of RM matrix + Ta_3Al_2CoC precipitate might have some damage tolerance, and the discovery of such a microstructure illustrates the potential of the alloy design strategy.

Acknowledgements

The authors acknowledge funding from Rolls-Royce plc and the EPSRC under the Rolls-Royce/EPSRC Strategic Partnership (EP/H022309/1). The raw research data associated with this work can be accessed via the following DOI: 10.5281/zenodo.2628789. The author(s) acknowledges the use of the School of Materials X-ray Diffraction Suite at the University of Manchester and is grateful for the technical support and data collected by Gary Harrison and Dr. John E. Warren.

Appendix A. Supplementary data

Supplementary data to this article can be found online at https://doi.org/10.1016/j.jallcom.2019.07.003.

References

[1] Advisory Council for Aeronautics Research in Europe (ACARE), European Commission, Flightpath 2050, Europe's Vision for Aviation, 2011.

[2] Rolls-Royce Plc, the Jet Engine, fifth ed., Wiley, 2005.
[3] H. Frost, M. Ashby, Deformation-mechanism Maps: the Plasticity and Creep of Metals and Ceramics, Pergamon Press, 1982.
[4] A. Brown, M. Ashby, Correlations for diffusion constants, Acta Metall. 28 (1980) 1085–1101.
[5] R. Fleischer, High-strength, high-temperature intermetallic compounds, J. Mater. Sci. 22 (1987) 2281–2288.
[6] K. Onal, M. Maris-Sida, G. Meier, F. Pettit, The effects of water vapor on the oxidation of nickel-base superalloys and coatings at temperatures from 700° to 1100°, in: K. Green, T. Pollock, H. Harada, T. Howson, R. Reed, J. Schirra, S. Walston (Eds.), Superalloys 2004, TMS, 2004, pp. 607–615.
[7] S. Saunders, M. Monteiro, F. Rizzo, The oxidation behaviour of metals and alloys at high temperatures in atmospheres containing water vapour: a review, Prog. Mater. Sci. 53 (2008) 775–837.
[8] ASM International. ASM Alloy Phase Diagram Database (accessed January 2017) [online].
[9] G. Gosh, G.B. Olson, Integrated design of Nb-based superalloys: ab initio calculations, computational thermodynamics and kinetics, and experimental results, Acta Mater. 55 (2007) 3281–3303.
[10] R. Ferro, A. Saccone, S. Delfino, Aluminium-cobalt-tantalum, in: Ternary Alloys, VCH, 1991, pp. 260–261.
[11] C. Hunt, A. Raman, Alloy chemistry of σ-related phases: I. Extension of μ and occurrence of μ'Phases in the ternary systems Nb (Ta)-X-Al (X= Fe, Co, Ni, Cu, Cr, Mo), Z. Metallkd 59 (1968) 701–707.
[12] O. Dovbenko, F. Stein, M. Palm, O. Prymak, Experimental determination of the ternary CoeAleNb phase diagram, Intermetallics 18 (2010) 2191–2207.
[13] E. Reiffenstein, H. Nowotny, F. Benesovsky, Einige neue η-Carbide, Monatsh. Chem. Verw. Teile Anderer Wiss. 96 (1965) 1543–1546.
[14] J. Etzkorn, H. Hillebrecht, Synthesis, crystal growth, and structure of Ta_3Al_2. CoC—an ordered quarternary cubic η-carbide and the first single crystal study of a η-carbide, J. Solid State Chem. 181 (2008) 1342–1346.
[15] A.B. Greninger, A.R. Troiano, The mechanism of martensite formation, Trans. Am. Inst. Min. Metall. Eng. 185 (1949) 590–598.
[16] G. Wassermann, Einfluss der α–γ-Umwandlung eines Irreversiblen Nickelstahls auf Kristallorientierung und Zugfestigkeit, Archive für das Eisenhüttenwesen 6 (1933) 347–351.
[17] Z. Nishiyama, X-Ray Investigation of the Mechanism of the Transformation from Face-Centred Cubic Lattice to Body-Centred Cubic vol. 23, Science Reports of the Tohoku Imperial University, 1934, pp. 637–673.
[18] U. Dahmen, Orientation relationships in precipitation systems, Acta Metall. 30 (1982) 63–73.